Plasma Chem Plasma Process (2012) 32:547–564
DOI 10.1007/s11090-012-9368-x

ORIGINAL PAPER

Numerical Investigation of a Parallel-Plate Atmospheric-Pressure Nitrogen/Ammonia Dielectric Barrier Discharge

F.-L. Li · K.-M. Lin · Y.-W. Yang · C.-T. Hung · J.-S. Wu · J.-P. Yu

Received: 26 November 2011 / Accepted: 23 March 2012 / Published online: 6 April 2012

Abstract In this paper, a planar atmospheric-pressure dielectric barrier discharge (AP-DBD) of nitrogen mixed with ammonia (0–2 %) is simulated using one-dimensional self-consistent fluid modeling with cell-centered finite-volume method. This AP-DBD is driven by a 30 kHz power source with distorted sinusoidal voltages. The simulated discharge current densities are found to be in good agreement with the experiment data in both phase and magnitude. The simulated results show that the discharges of N_2 mixed with NH_3 (0–2 %) are all typical Townsend-like discharges because the ions always outnumber the electrons very much which leads to no quasi-neutral region in the gap throughout the cycle. N_2^+ and N_4^+ are found to be the most abundant charged species during and after the breakdown process, respectively, like a pure nitrogen DBD. NH_4^+ increases rapidly initially with increasing addition of NH_3 and levels off eventually. In addition, N is the most dominant neutral species, except the background species, N_2 and NH_3, and NH_2 and H are the second dominant species, which increase with increasing added NH_3. The existence of abundant NH_2 plays an important role in those applications which require functional group incorporation.

Keywords Fluid modeling · Finite-volume method · Atmospheric-pressure dielectric barrier discharge · Nitrogen · Ammonia · Townsend-like discharge

F.-L. Li · K.-M. Lin · Y.-W. Yang · C.-T. Hung · J.-S. Wu (✉)
Department of Mechanical Engineering, National Chiao Tung University, Hsinchu, Taiwan
e-mail: chongsin@faculty.nctu.edu.tw

J.-S. Wu
National Center for High-Performance Computing, Hsinchu, Taiwan

J.-P. Yu
Department of Information Management, Ming Chuan University, Taoyuan, Taiwan

Introduction

Atmospheric-pressure plasmas (APP) have attracted much attention recently mainly because: (1) they do not require the use of expensive vacuum equipment, and (2) they have found increasingly numerous applications in modern science and technology. The former drives the cost down dramatically as compared with low-pressure plasmas and also offers the possibility of in-line processing for mass production in industry. The latter have led to development of different kinds of AP plasma sources. Among these APPs, dielectric barrier discharges (DBD) using ammonia have been well studied experimentally because it can produce abundant atomic nitrogen and hydrogen which are used in various applications such as surface treatment to improve wettability [1], biocompatibility of polymer surfaces [2], surface nitridation for semiconductor applications [3, 4], and modifying surfaces for increased adhesion between polymer layers in composite materials [5], among others. There exist several studies of AP-DBD with simulations [nitrogen: 6–8; helium: 9–12] and experiments [nitrogen: 13–15; helium: 14]. However, nearly no related simulation study in ammonia DBD has been found, except very few in low-pressure environments for DBD [4] and ICP [16].

Recently, nitrogen/ammonia plasma has also been studied experimentally in low-pressure environment because of its potential applications, such as surface nitridation for semiconductor applications [3, 17], etching [18–20], reduction of nitrogen oxide [21], modification of surface wetting properties [22] and laser [23]. There have been very few experimental studies of AP-DBD for nitrogen/ammonia mixture [e.g., 24]. Recently, we have developed a two-step AP plasma treatment for increasing the bio-compatibility of Polylactide (PLA) [25, 26]: first by nitrogen/oxygen DBD and followed by nitrogen/ammonia DBD. Results had shown that appreciable amount of N1 s and NH_2 bond were incorporated into PLA surface after the two-step plasma treatment process. However, no detailed physical and chemical mechanisms of nitrogen/oxygen and nitrogen/ammonia discharges were provided, especially the latter. Thus, better understanding of nitrogen/ammonia AP-DBD is strongly desired.

It is well known that detailed experimental measurement of the discharge is not an easy task. Plasma fluid modeling may represent one of the cheapest and most effective tools in unveiling the insight of complex physics and chemistry in nitrogen/ammonia AP-DBD. Hopefully, much deeper understanding of the plasma mechanism can provide more constructive input to the design of plasma source. Unfortunately, there has been no related simulation study on N_2/NH_3 AP-DBD to the best knowledge of the authors.

In the current study, the structure of a parallel-plate nitrogen/ammonia AP-DBD is simulated using a previously developed 1-D fluid modeling code. The fluid modeling code is first validated by good agreement of discharge current densities between simulations and experiments. Then, effect of ammonia addition into nitrogen on the structure of gas discharge is presented and discussed in detail. Finally, important findings are summarized at the end of the paper.

Numerical Method

Fluid Modeling Equations

The governing equations for the fluid modeling of plasma are the same as our previous work [27], which was based on LMEA (local mean energy approximation) approach [28],

and are briefly described below for completeness. The general continuity equation for ion species can be written as

$$\frac{\partial n_p}{\partial t} + \vec{\nabla} \cdot \vec{\Gamma}_p = \sum_{i=1}^{r_p} S_{p_i} \quad p = 1, \ldots, K \tag{1}$$

where n_p is the number density of ion species p, K is the number of ion species, r_p is the number of reaction channels that involve the creation and destruction of ion species p and $\vec{\Gamma}_p$ is the particle flux that is expressed, based on the drift–diffusion approximation, as

$$\vec{\Gamma}_p = \text{sign}(q_p)\mu_p n_p \vec{E} - D_p \vec{\nabla} n_p \tag{2}$$

$$\vec{E} = -\vec{\nabla}\phi \tag{3}$$

where q_p, $\vec{E}$, ϕ, μ_p, and D_p are the ion charge, the electric field, the electric potential, the ion mobility, and the ion diffusivity respectively. Note that the form of the source term S_{p_i} can be modified according to the modeled reactions describing how the ion species p is generated or destroyed in reaction channel i.

The continuity equation for electron species can be written as

$$\frac{\partial n_e}{\partial t} + \vec{\nabla} \cdot \vec{\Gamma}_e = \sum_{i=1}^{r_e} S_{e_i} \tag{4}$$

where n_e is the number density of electrons, r_e is the number of reaction channels that involve the creation and destruction of electrons and $\vec{\Gamma}_e$ is the corresponding particle flux that is expressed, based on drift–diffusion approximation, as

$$\vec{\Gamma}_e = -\mu_e n_e \vec{E} - D_e \vec{\nabla} n_e \tag{5}$$

where μ_e and D_e are the electron mobility and electron diffusivity, respectively. These two transport coefficients can be readily obtained as a function of the electron temperature from the solution of a publicly available computer code for the Boltzmann equation, named BOLSIG$^+$ [29]. Similar to S_{P_i}, the form of S_{e_i} can also be modified according to the modeled reactions that generate or destroy the electron in reaction channel i.

The continuity equation for neutral species can be written as

$$\frac{\partial n_{uc}}{\partial t} + \vec{\nabla} \cdot \vec{\Gamma}_{uc} = \sum_{i=1}^{r_{uc}} S_{uc_i} \quad uc = 1, \ldots, L \tag{6}$$

where n_{uc} is the number density of uncharged neutral species uc, L is the number of neutral species, r_{uc} is the number of reaction channels that involve the generation and destruction of uncharged species uc and $\vec{\Gamma}_{uc}$ is the corresponding particle flux, neglecting convection effects, which can be expressed as

$$\vec{\Gamma}_{uc} = -D_{uc} \vec{\nabla} n_{uc} \tag{7}$$

where D_{uc} is the diffusivity of neutral species. Similarly, the form of S_{uc_i} can also be modified according to the modeled reactions that generate or destroy the neutral species in reaction channel i.

The electron energy density equation can be expressed as

$$\frac{\partial n_\varepsilon}{\partial t} + \vec{\nabla} \cdot \vec{\Gamma}_{n_\varepsilon} = -e\vec{\Gamma}_e \cdot \vec{E} - \sum_{i=1}^{S_c} \varepsilon_i k_i n_i - 3\frac{m_e}{M} n_e k_B \nu_m \left(T_e - T_g\right) \tag{8}$$

where $n_\varepsilon \left(= \frac{3}{2} n_e k_B T_e\right)$ is the electron energy density, T_e is the electron temperature, ε_i and k_i are the energy loss and rate constant for the ith inelastic electron collision respectively, $S_c$is the number of reaction channels of inelastic electron collision, k_B is the Boltzmann constant, ν_m is the momentum exchange collision frequency between the electron (mass m_e) and the background neutral (mass M), T_g is the background gas temperature and is assumed to be 400 K. $\vec{\Gamma}_{n_\varepsilon}$ is the corresponding electron energy density flux and can be expressed as

$$\vec{\Gamma}_{n_\varepsilon} = \frac{5}{2} k_B T_e \vec{\Gamma}_e - \frac{5}{2} D_e n_e \vec{\nabla}(k_B T_e) \tag{9}$$

The second term on the right-hand side of Eq. 8 represents the sum of the energy losses of the electrons due to inelastic collision with other species. The last term on the right-hand side of Eq. 8 can be ignored for low-pressure gas discharges, while it is important for medium-to-atmospheric pressure discharges.

The Poisson equation for electrostatic potential can be expressed as

$$\vec{\nabla} \cdot (\varepsilon \vec{\nabla} \phi) = -\sum_{i=1}^{K} (qn)_i \tag{10}$$

where ϕ is the potential and ε is a function of position, whose value is either the vacuum or dielectric permittivity.

Discretization, Numerical Schemes and Algorithms

In the current study, the above equations are discretized using the collocated cell-centered finite-volume method [30]. Details are presented elsewhere [31] and only several key features are described here for brevity. The fluxes in the continuity equations and the electron energy density equation are evaluated using the Scharfetter–Gummel scheme [32]. At each time step, the resulting algebraic linear systems are solved equation by equation using parallel preconditioned Krylov subspace method provided by PETSc library [33] through domain decomposition technique on top of the MPI protocol. We have employed the additive Schwarz method, with LU or incomplete LU as a sub-domain solver, for preconditioning the coefficient matrix and then the GMRES (Generalized Minimal Residual Method) [34] for solving the linear matrix equation.

Boundary Conditions

The flux-type boundary conditions of ions, electrons, and neutral species are employed on the solid surfaces (dielectric or electrode) as

$$\vec{\Gamma}_p = a \cdot sign(q_p) \mu_p n_p \vec{E} - D_p \vec{\nabla} n_p \tag{11}$$

$$\vec{\Gamma}_e = -a \cdot \mu_e n_e \vec{E} - D_e \vec{\nabla} n_e + \frac{1}{4} n_e \nu_{th} \tag{12}$$

$$\vec{\Gamma}_{uc} = -D_{uc}\vec{\nabla}n_{uc} \tag{13}$$

where $a = 1$ if drift velocity $(sign(q_p)\mu_p\vec{E})$ points toward the dielectric surface, and $a = -1$ otherwise. The ions and electrons are assumed to be accumulated at the dielectric surface at the boundary, while the neutral species are assumed to be quenched at the dielectric surface in the present study. The thermal velocity of electron is

$$v_{th} = \sqrt{\frac{8k_BT_e}{\pi m_e}} \tag{14}$$

where m_e is the electron mass. Note that the effect of secondary electron emission is neglected since we have found that it is not important in current study by varying the coefficient of secondary electron emission in the range of 0.001–0.1.

The boundary conditions of electron energy density flux at the dielectric surfaces are

$$\vec{\Gamma}_{n_\varepsilon} = 2k_BT_e\vec{\Gamma}_e \tag{15}$$

For the Poisson equation, the potentials of powered and grounded electrode are assigned with applied voltage and zero potential respectively.

Plasma Chemistry

In the plasma chemistry, we consider 23 species (e^-, NH^+, NH_2^+, NH_3^+, NH_4^+, N^+, N_2^+, N_4^+, H^+, H_2^+, N^*, N_2^*, NH, NH_2, N_2H, N_2H_3, N, H, N_2H_2, N_2H_4, H_2, N_2, and NH_3) and 142 reaction channels as summarized in Tables 1, 2, and 3, which include 56 electron-impact reactions, 35 ion-molecular reactions and 51 neutral–neutral reactions respectively. Reaction channels 1–22 consider chemistry for the pure ammonia discharge, reaction channels 23–43 consider chemistry for the pure nitrogen discharge, reaction channels 44–56 consider chemistry for the pure hydrogen discharge, while the rest consider chemistry among the species. This set of nitrogen/ammonia plasma chemistry includes momentum transfer collision, electron-impact vibrational excitation, electron-impact rotational excitation, electron-impact electronic excitation, electron-impact ionization, electron-impact dissociation, electron-impact dissociative ionization, electron–ion recombination, electron–ion dissociative recombination, ion-molecular charge exchange, ion-molecular metastable into ground state, and metastable–metastable associative ionization.

Results and Discussion

Simulation Conditions

Figure 1 illustrates the schematic diagram of the one-dimensional atmospheric-pressure dielectric barrier discharge (AP-DBD). The discharge is sustained in the 1-mm gap between two electrodes (50 × 50 mm each) with each covered by a 1-mm thick quartz plate having measured relative permittivity of 4.76. The powered electrode (left) is driven by a 30 kHz power source with distorted sinusoidal voltages of 8 kV in amplitude, and the right electrode is grounded throughout the cycle. This configuration is kept the same through the study. Effect of ammonia addition in the range of 0–2 % is considered in the simulations. 130 cells with non-uniform spacing were found to be accurate enough after detailed grid convergence study and were used throughout the study. Time step is set as

Table 1 Electron-impact collisions include nitrogen/ammonia plasma chemistry

No	Reaction	Threshold energy (eV)	Reaction type	References
1	$NH_3 + e^- \rightarrow NH_3 + e^-$	0.0	Momentum	[16]
2	$NH_3 + e^- \rightarrow NH_3 + e^-$	0.12	Vibrational excitation	[16]
3	$NH_3 + e^- \rightarrow NH_3 + e^-$	0.2	Vibrational excitation	[16]
4	$NH_3 + e^- \rightarrow NH_3 + e^-$	0.42	Vibrational excitation	[16]
5	$NH_3 + e^- \rightarrow NH_2 + H + e^-$	5.72	Dissociation	[16]
6	$NH_3 + e^- \rightarrow NH + H + H + 2e^-$	8.65	Dissociation	[16]
7	$NH_3 + e^- \rightarrow NH_3^+ + 2e^-$	10.2	Ionization	[16]
8	$NH_3 + e^- \rightarrow NH_2^+ + H + 2e^-$	16.0	Dissociative ionization	[16]
9	$NH_2 + e^- \rightarrow NH_2 + e^-$	0.0	Momentum	[16]
10	$NH_2 + e^- \rightarrow NH_2 + e^-$	0.12	Vibrational excitation	[16]
11	$NH_2 + e^- \rightarrow NH_2 + e^-$	0.2	Vibrational excitation	[16]
12	$NH_2 + e^- \rightarrow NH_2 + e^-$	0.42	Vibrational excitation	[16]
13	$NH_2 + e^- \rightarrow NH + H + e^-$	5.72	Dissociation	[16]
14	$NH_2 + e^- \rightarrow N + H + H + 2e^-$	8.65	Dissociation	[16]
15	$NH_2 + e^- \rightarrow NH_2^+ + 2e^-$	11.14	Ionization	[16]
16	$NH_2 + e^- \rightarrow NH^+ + H + 2e^-$	17.6	Dissociative ionization	[16]
17	$NH + e^- \rightarrow NH + e^-$	0.0	Momentum	[16]
18	$NH + e^- \rightarrow NH + e^-$	0.12	Vibrational excitation	[16]
19	$NH + e^- \rightarrow NH + e^-$	0.2	Vibrational excitation	[16]
20	$NH + e^- \rightarrow NH + e^-$	0.42	Vibrational excitation	[16]
21	$NH + e^- \rightarrow N + H + e^-$	5.72	Dissociation	[16]
22	$NH + e^- \rightarrow NH^+ + 2e^-$	13.49	Ionization	[16]
23	$N_2 + e^- \rightarrow N_2 + e^-$	0.0	Momentum	[16]
24	$N_2 + e^- \rightarrow N_2 + e^-$	0.02	Rotational excitation	[16]
25	$N_2 + e^- \rightarrow N_2 + e^-$	0.291	Vibrational exication	[16]
26	$N_2 + e^- \rightarrow N_2 + e^-$	0.59	Vibrational exication	[16]
27	$N_2 + e^- \rightarrow N_2 + e^-$	0.88	Vibrational exication	[16]
28	$N_2 + e^- \rightarrow N_2 + e^-$	1.47	Vibrational exication	[16]
29	$N_2 + e^- \rightarrow N_2 + e^-$	1.76	Vibrational exication	[16]
30	$N_2 + e^- \rightarrow N_2 + e^-$	2.06	Vibrational exication	[16]
31	$N_2 + e^- \rightarrow N_2 + e^-$	2.35	Vibrational exication	[16]
32	$N_2 + e^- \rightarrow N_2^* + e^-$	6.17	Electronic exication	[16]
33	$N_2 + e^- \rightarrow N_2^* + e^-$	7.0	Electronic excitation	[16]
34	$N_2 + e^- \rightarrow N_2^* + e^-$	7.35	Electronic excitation	[16]
35	$N_2 + e^- \rightarrow N_2^* + e^-$	8.16	Electronic excitation	[16]
36	$N_2 + e^- \rightarrow N_2^* + e^-$	8.4	Electronic excitation	[16]
37	$N_2 + e^- \rightarrow N_2^* + e^-$	11.03	Electronic excitation	[16]
38	$N_2 + e^- \rightarrow N + N + e^-$	13.0	Dissociation	[16]
39	$N_2 + e^- \rightarrow N_2^+ + 2e^-$	15.8	Ionization	[16]
40	$N + e^- \rightarrow N + e^-$	0.0	Momentum	[16]
41	$N + e^- \rightarrow N^* + e^-$	2.38	Electronic excitation	[16]
42	$N + e^- \rightarrow N^* + e^-$	3.58	Electronic excitation	[16]
43	$N + e^- \rightarrow N^+ + 2e^-$	14.54	Ionization	[16]

Table 1 continued

No	Reaction	Threshold energy (eV)	Reaction type	References
44	$H_2 + e^- \rightarrow H_2 + e^-$	0.0	Momentum	[16]
45	$H_2 + e^- \rightarrow H_2 + e^-$	0.044	Rotational excitation	[16]
46	$H_2 + e^- \rightarrow H_2 + e^-$	0.073	Rotational excitation	[16]
47	$H_2 + e^- \rightarrow H_2 + e^-$	0.516	Vibrational excitation	[16]
48	$H_2 + e^- \rightarrow H_2 + e^-$	1.0	Vibrational excitation	[16]
49	$H_2 + e^- \rightarrow H_2 + e^-$	1.5	Vibrational excitation	[16]
50	$H_2 + e^- \rightarrow H_2 + e^-$	11.3	Electronic excitation	[16]
51	$H_2 + e^- \rightarrow H_2 + e^-$	11.75	Electronic excitation	[16]
52	$H_2 + e^- \rightarrow H_2 + e^-$	11.8	Electronic excitation	[16]
53	$H_2 + e^- \rightarrow H_2 + e^-$	12.4	Electronic excitation	[16]
54	$H_2 + e^- \rightarrow H_2 + e^-$	14.0	Electronic excitation	[16]
55	$H_2 + e^- \rightarrow H + H + e^-$	8.9	Dissociation	[16]
56	$H_2 + e^- \rightarrow H_2^+ + 2e^-$	15.43	Ionization	[16]

All rate constants are adopted from [29, 40]

10^{-10}–10^{-11} s, unless otherwise specified. The electrical properties of the discharges remain essentially the same after 3–5 cycles of simulation, although the neutral species are still evolving slightly. Thus, we have used the results obtained at 5th cycle throughout the paper.

Validation with Experimental Results

Figure 2 shows the comparison of simulated discharge current densities generated by a pure nitrogen AP-DBD with the experimental data obtained in this study. Detailed description of the experimental setup can be found in Chiang et al. [35] and are not repeated here for brevity. Note the simulated voltage waveform was fitted using 30 terms of Fourier series expansion with 30 kHz as the fundamental frequency. On top of the figure, there is a photo taken from the bottom of the discharge with 0.2 s of exposure time. It shows that the discharge is very uniform in the direction parallel to the plates, which may justify the use of 1-D fluid modeling in the current study. Similar homogeneous DBDs with nitrogen at atmospheric condition were also found in several previous experimental and numerical studies [36–37 and references cited therein]. Results show that the simulated discharge current densities are in excellent agreement with the measurements quantitatively. This may be attributed to the LMEA approach adopted in the current fluid modeling, which has demonstrated better agreement with measurements for low-pressure gas discharge [28], although it is atmospheric in the current study. Similarly, the discharge current densities for the cases of 0.1 and 2.0 % addition of NH_3 are found to agree well with the experiments. In general, the addition of NH_3 into the nitrogen AP-DBD does not influence the discharge current densities very much based on the simulations and experiments, although the visible light emission becomes dimmer with increasing concentration of NH_3. The dimmer light emission with increasing ammonia amount may possibly be attributed to less emission of photons resulting from, e.g., $N_2(B^3\Pi_g)$ to $N_2(A^3\Sigma_u^+)$ (580 nm) and makes the photo much dimmer. Unfortunately, we have not considered different excited and

Table 2 Ion-molecular collisions include nitrogen/ammonia plasma chemistry

No	Reaction	Rate constant ($cm^3\ s^{-1}$)	References
1	$N_2^+ + N \rightarrow N^+ + N_2$	5.0×10^{-12}	[16]
2	$N_2^+ + N^* \rightarrow N^+ + N_2$	1.0×10^{-10}	[16]
3	$N_2^+ + N^* \rightarrow N_2^+ + N_2$	1.0×10^{-9}	[16]
4	$N_2^+ + N_2^* \rightarrow N_2^+ + N_2$	1.0×10^{-9}	[16]
5	$N_4^+ + e^- \rightarrow N_2^* + N_2$	$2.0 \times 10^{-6}(T_g/T_e)^{0.5}$	[7]
6	$N^+ + N \rightarrow N^+ + N$	1.0×10^{-9}	[16]
7	$N^+ + N^* \rightarrow N^+ + N$	1.0×10^{-9}	[16]
8	$N^+ + N_2 \rightarrow N^+ + N_2$	1.0×10^{-9}	[16]
9	$N^+ + N_2^* \rightarrow N^+ + N_2$	1.0×10^{-9}	[16]
10	$H_2^+ + NH_3 \rightarrow NH_3^+ + H_2$	4.4×10^{-9}	[16]
11	$H_2^+ + NH \rightarrow NH^+ + H_2$	5.0×10^{-10}	[16]
12	$H_2^+ + NH \rightarrow NH_2^+ + H$	5.0×10^{-11}	[16]
13	$H_2^+ + NH_2 \rightarrow NH_2^+ + H_2$	5.0×10^{-10}	[16]
14	$H_2^+ + NH_2 \rightarrow NH_3^+ + H$	5.0×10^{-11}	[16]
15	$H_2^+ + NH_3 \rightarrow NH_3^+ + H_2$	5.7×10^{-9}	[16]
16	$H_2^+ + NH_3 \rightarrow NH_4^+ + H$	5.0×10^{-11}	[16]
17	$H^+ + NH_3 \rightarrow NH_3^+ + H$	5.0×10^{-11}	[16]
18	$H^+ + NH_2 \rightarrow NH_2^+ + H$	5.0×10^{-11}	[16]
19	$H^+ + NH \rightarrow NH^+ + H$	5.0×10^{-11}	[16]
20	$NH^+ + NH_3 \rightarrow NH_3^+ + NH$	2.4×10^{-9}	[16]
21	$NH^+ + NH_3 \rightarrow NH_4^+ + N$	1.8×10^{-9}	[16]
22	$NH^+ + H_2 \rightarrow NH_2^+ + H$	1.0×10^{-9}	[16]
23	$NH_2^+ + NH_3 \rightarrow NH_3^+ + NH_2$	2.2×10^{-9}	[16]
24	$NH_2^+ + NH_3 \rightarrow NH_4^+ + NH$	2.2×10^{-9}	[16]
25	$NH_2^+ + H_2 \rightarrow NH_3^+ + H$	1.0×10^{-9}	[16]
26	$NH_3^+ + NH_3 \rightarrow NH_4^+ + NH_2$	2.2×10^{-9}	[16]
27	$NH_3^+ + H_2 \rightarrow NH_4^+ + H$	4.0×10^{-13}	[16]
28	$NH_3^+ + H_2 \rightarrow H_2^+ + NH_3$	9.63×10^{-13} $(T_g/298)^{-0.25}\exp(-14.6/T_g)$	[16]
29	$NH_3^+ + NH_3 \rightarrow H^+ + NH_2 + NH_3$	6.87×10^{-10} $(T_g/298)^{-0.17}\exp(-4.6/T_g)$	[16]
30	$NH_3^+ + H_2 \rightarrow H_2^+ + NH_2 + H$	2.18×10^{-9} $(T_g/298)^{-0.2}\exp(-9.9/T_g)$	[16]
31	$NH_3^+ + NH_3 \rightarrow NH_2^+ + H_2 + NH_2$	6.12×10^{-7} $(T_g/298)^{-0.44}\exp(-3.8/T_g)$	[16]
32	$NH_3^+ + H_2 \rightarrow H^+ + NH_3 + H$	8.46×10^{-10} $(T_g/298)^{-0.39}\exp(-14.8/T_g)$	[16]
33	$NH_4^+ + e^- \rightarrow NH_3 + H$	$9.0 \times 10^{-7}T_e^{-0.6}$	[4]
34	$H^+ + H_2 \rightarrow H_2^+ + H$	$3.22 \times 10^{-10} \times \exp(21{,}856/T_g)$	[16]
35	$H_2^+ + H \rightarrow H^+ + H$	6.40×10^{-10}	[16]

T_e is the electron temperature, and T_g is the background gas temperature. Both are in Kevin

Table 3 Neutral-neutral collisions include nitrogen/ammonia plasma chemistry

No	Reaction	Rate constant			References
		k_0 ($cm^3\ s^{-1}$)	n	E_a/R (K)	
1	$NH_3 + H \rightarrow H_2 + NH_2$	1.34×10^{-10}	0	7,352	[16]
2	$NH_3 + NH + M \rightarrow N_2H_4 + M$	5.0×10^{-35}	0	0	[16]
3	$NH_2 + H \rightarrow H_2 + NH$	4.81×10^{-12}	0	0	[16]
4	$NH_2 + H_2 \rightarrow H + NH_3$	2.09×10^{-12}	0	4,277	[16]
5	$NH_2 + NH_2 \rightarrow H_2 + N_2H_2$	8.31×10^{-11}	0	0	[16]
6	$NH_2 + NH_2 \rightarrow NH_3 + NH$	8.31×10^{-11}	0	5,100	[16]
7	$NH_2 + N \rightarrow N_2 + H + H$	1.2×10^{-10}	0	0	[16]
8	$NH_2 + NH \rightarrow H + N_2H_2$	2.49×10^{-9}	−0.5	0	[16]
9	$NH_2 + NH \rightarrow N_2H_3$	1.16×10^{-10}	0	0	[16]
10	$NH + N \rightarrow N_2 + H$	2.5×10^{-11}	0	0	[16]
11	$NH_2 + NH + M \rightarrow NH_3 + M$	6.06×10^{-30}	0	0	[16]
12	$NH + H \rightarrow H_2 + N$	5.98×10^{-11}	0	166	[16]
13	$NH + H_2 \rightarrow H + NH_2$	5.96×10^{-11}	0	7,782	[16]
14	$NH + NH \rightarrow N_2 + H + H$	1.16×10^{-9}	0	0	[16]
15	$NH + NH \rightarrow N_2H_2$	3.49×10^{-12}	0	0	[16]
16	$NH + NH \rightarrow NH_2 + N$	1.40×10^{-14}	2.89	−1,015	[16]
17	$N + H_2 \rightarrow NH + H$	2.66×10^{-10}	0	12,609	[16]
18	$H + H + NH_3 \rightarrow H_2 + NH_3$	1.40×10^{-31}	0	0	[16]
19	$H + H + NH_2 \rightarrow H_2 + NH_2$	1.40×10^{-31}	0	0	[16]
20	$N + H + NH_3 \rightarrow NH + NH_3$	5.00×10^{-32}	0	0	[16]
21	$H + N + H \rightarrow H + NH$	5.00×10^{-32}	0	0	[16]
22	$H + NH_2 + NH_3 \rightarrow NH_3 + NH_3$	6.00×10^{-30}	0	0	[16]
23	$N + H + H \rightarrow NH + H$	5.00×10^{-32}	0	0	[16]
24	$H + NH_2 + H \rightarrow H + NH_3$	6.00×10^{-30}	0	0	[16]
25	$H + NH_2 + NH_2 \rightarrow NH_3 + NH_2$	6.00×10^{-30}	0	0	[16]
26	$N_2H_2 + H \rightarrow N_2 + H + H_2$	4.53×10^{-13}	2.63	−115	[16]
27	$N_2H_2 + NH_2 \rightarrow N_2 + H + NH_3$	1.53×10^{-13}	4.05	−810.7	[16]
28	$N_2H_3 + H \rightarrow NH_2 + NH_2$	2.66×10^{-12}	0	0	[16]
29	$N_2H_3 + N_2H_3 \rightarrow NH_3 + NH_3 + N_2$	5.0×10^{-12}	0	0	[16]
30	$N_2H_3 + N_2H_3 \rightarrow N_2H_4 + N_2H_2$	2.0×10^{-11}	0	0	[16]
31	$N_2H_4 + N \rightarrow NH_2 + N_2H_2$	1.25×10^{-13}	0	0	[16]
32	$N_2H_4 + H \rightarrow N_2H_3 + H_2$	1.17×10^{-13}	0	1260.5	[16]
33	$N_2H_4 + NH_2 \rightarrow NH_3 + N_2H_3$	5.15×10^{-13}	0	0	[16]
34	$N_2H_2 + H \rightarrow N_2H + H_2$	8.31×10^{-11}	0	510	[16]
35	$N_2H_2 + NH \rightarrow N_2H + NH_2$	1.66×10^{-11}	0	510	[16]
36	$N_2H_2 + NH_2 \rightarrow N_2H + NH_3$	1.66×10^{-11}	0	510	[16]
37	$N_2H + H \rightarrow N_2 + H_2$	6.64×10^{-11}	0	1,531	[16]
38	$N_2H + NH \rightarrow N_2 + NH_2$	8.31×10^{-11}	0	0	[16]
39	$N_2H + NH_2 \rightarrow N_2 + NH_3$	8.31×10^{-11}	0	0	[16]
40	$N_2^* + N_2 \rightarrow N_2 + N_2$	1.9×10^{-13}	0	0	[16]
41	$N_2^* + N \rightarrow N + N_2$	1.0×10^{-13}	0	0	[16]
42	$N_2^* + N^* \rightarrow N + N_2$	1.0×10^{-13}	0	0	[16]

Table 3 continued

No	Reaction	Rate constant			References
		k_0 ($cm^3\ s^{-1}$)	n	E_a/R (K)	
43	$N^* + N_2 \rightarrow N + N_2$	2.0×10^{-14}	0	0	[16]
44	$N^* + N + M \rightarrow N_2^* + M$	2.0×10^{-32}	0	0	[16]
45	$N + N + M \rightarrow N_2^* + M$	1.0×10^{-32}	0	0	[16]
46	$N + N + M \rightarrow N_2 + M$	1.0×10^{-32}	0	0	[16]
47	$N_2^* + N_2 \rightarrow N_2 + N_2^*$	1.36×10^{-9}	0	0	[16]
48	$N_2 + N_2 \rightarrow N + N + N_2$	4.29×10^{-10}	0	86,460	[16]
49	$N_2^* + N_2^* \rightarrow N_4^+ + e^-$	2.0×10^{-10}	0	0	[7]
50	$H + H + N_2 \rightarrow H_2 + N_2$	1.9×10^{-31}	−1.32	0	[16]
51	$H + H + M \rightarrow H_2 + M$	1.9×10^{-31}	−0.06	0	[16]

The rate constants are calculated by $k = k_0 \times (T_g/298)^n \times \exp(-E_a/R\ T_g)$ where T_g is the background gas temperature (K)

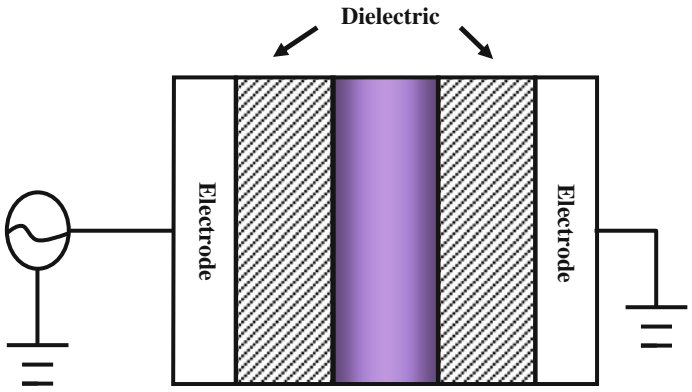

Fig. 1 Schematic diagram of one-dimensional atmospheric pressure dielectric barrier discharge

metastable states in the current study because the rate constant data are not available for their reactions with ammonia. Thus, we have lumped all these together as N_2* in the modeling.

Effect of Ammonia Addition into Nitrogen AP-DBD

Figure 3 shows the cycle-space-averaged number densities of various charged species as a function of different concentrations of ammonia addition in a nitrogen AP-DBD. Results show that charged species such as electron, N_2^+ and N_4^+ are essentially the same with ammonia addition in the range of 0–2 %, which leads to the approximately the same discharge current densities. In addition, N_2^+ is the most dominant charged species and is at least two orders of magnitude more than electron, which is a typical feature of Townsend-like discharge. In the current study, the electric field is slightly increased from anode to cathode, much more ions than electrons, much more electrons near the anode, and currently density is relatively high ($\sim$10 mA/cm^2), which is termed as "Townsend-like

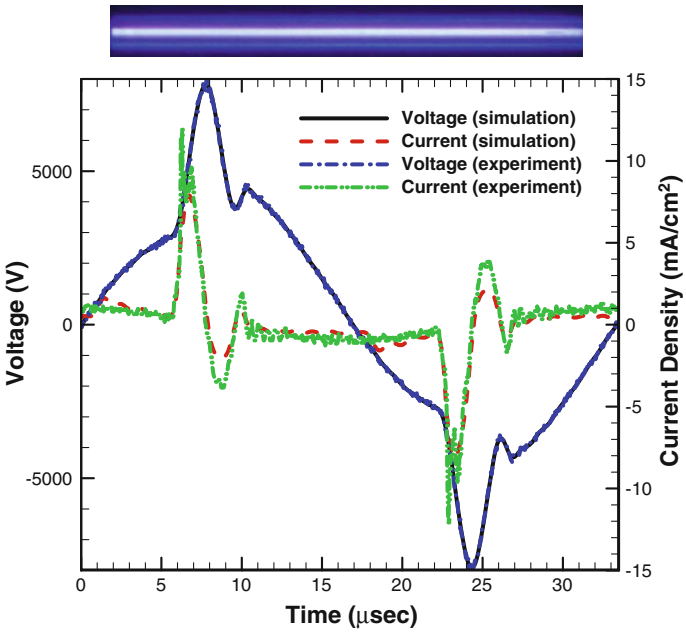

Fig. 2 Comparison of simulated and experimental current density in pure nitrogen AP-DBD

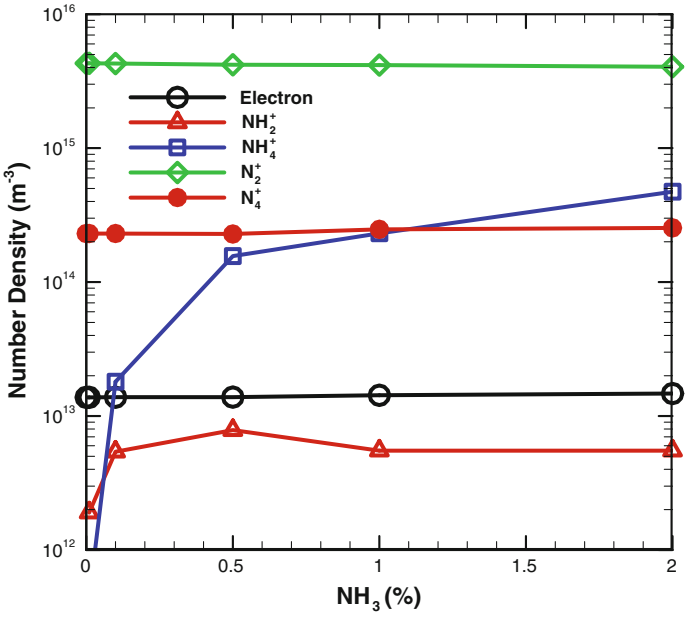

Fig. 3 Cycle-space-averaged number densities of charge species with concentration ratio of ammonia in AP-DBD

discharge". For the ammonia reaction related charged species, such as NH_4^+ and NH_2^+, their concentrations generally increase with increasing addition of ammonia and become roughly the same after 0.5 % of ammonia addition. In brief summary, the order of decreasing amount of charged species is $N_2^+ > N_4^+ > N_e > NH_2^+ > NH_4^+$ and $N_2^+ > N_4^+ > NH_4^+ > N_e > NH_2^+$ at smaller and larger ammonia addition respectively.

Figure 4 shows the temporal profiles of space-averaged number densities of charged species of nitrogen AP-DBD with 0.1 % ammonia addition. Results demonstrate that the number density of electron is always much smaller than the total number density of ions (N_2^+ and N_4^+) and is nearly the same as NH_4^+ during the gas breakdown period throughout a cycle. The simulated electric field across the gap is almost linear with slight distortion by the charge density during the breakdown period, which will be shown later (Fig. 6). The above two phenomena demonstrate that it is a typical Townsend-like discharge [7, 38], in which there is no quasi-neutral region and very weak (slightly non-constant) electric field in the gap. In addition, N_2^+ is found to be most during the breakdown process, while N_4^+ becomes dominant during the post-breakdown process due to associative ionization between metastable nitrogen generated during the breakdown process. NH_4^+ is found to be secondly dominant after the breakdown caused by the charge exchange between NH_x^+ ($x = 1$, 2, and 3) ions, leading to the formation of NH_4^+, which has the smallest ionization potential among all the ions in the chemical reaction channels. However, the NH_4^+ is not shown because of low quantity as compared with other.

In addition, Fig. 5 shows the temporal profiles of space-averaged number densities of neutral species of nitrogen AP-DBD with 0.1 % ammonia addition in a cycle. Results show that all neutral species change very little with time except metastable nitrogen throughout a cycle. Metastable nitrogen has changed dramatically with time, which is caused by excitation of electron impact on ground N_2 (No. 32–37 in Table 1), excited recombination of

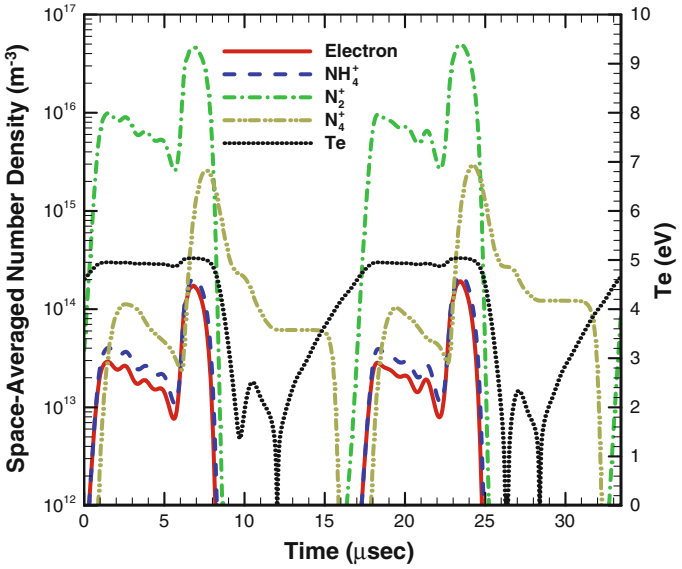

Fig. 4 The temporal profiles of space-averaged number densities of charge species for N_2/0.1 % NH_3 AP-DBD

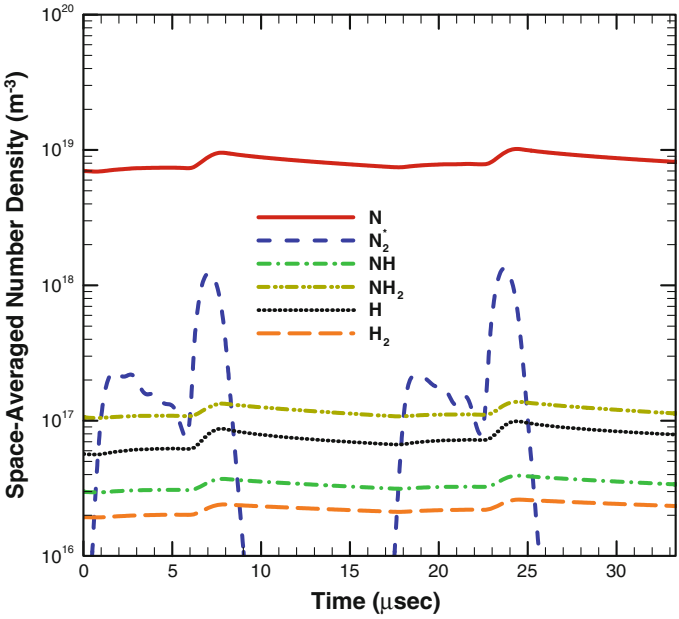

Fig. 5 The temporal profiles of space-averaged number densities of neutral species for N_2/0.1 % NH_3 AP-DBD

electron–ion on N_4^+ (No. 5 in Table 2), excited recombination, and exchange of neutral–neutral collision (No. 44, 45, and 47 in Table 3).

In Figs. 4 and 5, the electrical properties of the discharges reach a quasi-steady state at 3–5 cycles. It is because diffusion time scale is much longer than drift time scale due to electric field for charged species. It is also true that densities of neutral species increase slightly with time except the metastable species because of its very short life time. Thus, it is difficult for the neutral species to reach the "real" quasi-steady state within such a short period of physical time (3–5 cycles) in the simulation. However, the structure of discharge remains essentially unchanged even when the neutral species reach equilibrium after very long period of simulation.

Figures 6 and 7 show that the snapshots of distribution of charged species at the peak of the breakdown (highest discharge current density) and after the breakdown, respectively, which further reveals that nitrogen DBD is a typical Townsend-like discharge with addition of 0.1 % NH_3 as mentioned earlier. These two plots both show that ions outnumber electrons throughout the cycle. During the breakdown period, the electric field is almost linear (3–3.5 kV/mm) with slight distortion due to ion space charge and the electron temperature is roughly 5 eV. All the above show that it is a typical Townsend-like discharge as presented by other authors [7, 38]. In the post-breakdown period, only a very small amount of N_4^+ exists, resulting from the associative ionization of metastable/metastable nitrogen, with nearly a traced amount of electrons. Note the amounts of electron, N_2^+ and NH_4^+ are all very low which are not included in Fig. 7. The corresponding electric field is almost constant with a smaller value ($\sim$1 kV/mm), which mimics a capacitor without charged particles.

Figures 8 and 9 show the spatio-temporal evolution of number density of electron and N_2^+ along with the temporal simulated current density in a cycle. They show that electrons

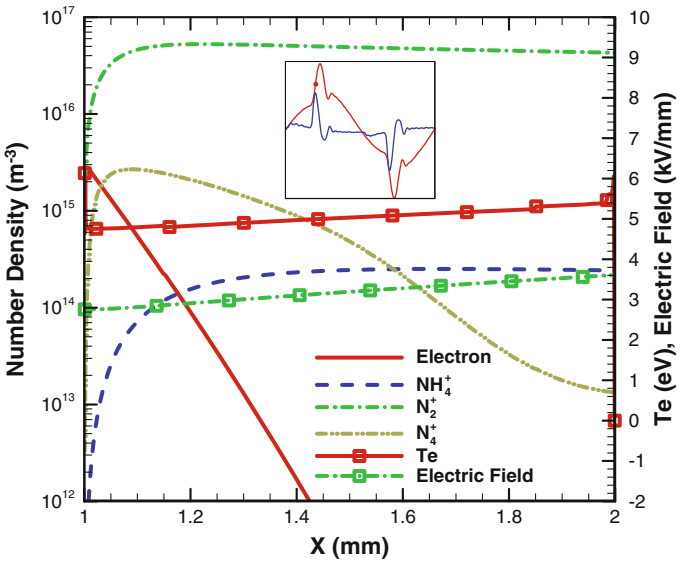

Fig. 6 Distribution of charge species densities across the electrode gap for N_2/0.1 % NH_3 AP-DBD at the peak of discharge current density

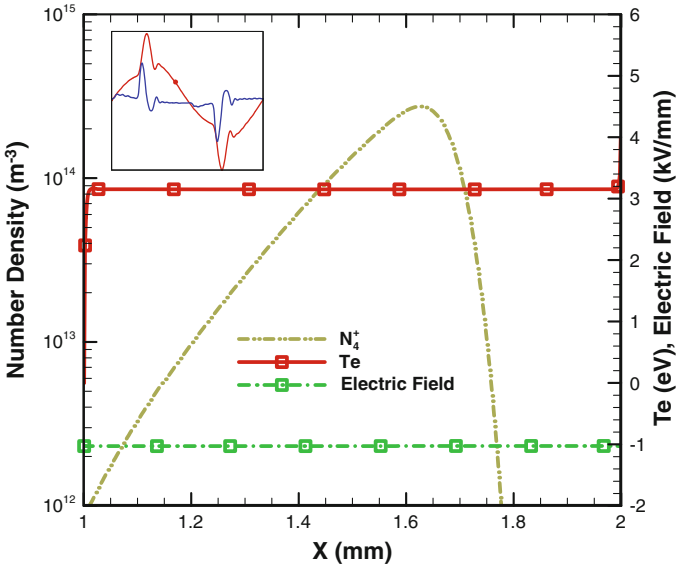

Fig. 7 Distribution of charge species densities across the electrode gap for N_2/0.1 % NH_3 AP-DBD in the post-breakdown period

are concentrated near the anode ($x = 1$ mm) and the ions (N_2^+) is relatively uniform across the gap. It clearly shows that ions outnumber electrons very much during the breakdown period near the cathode dielectric surface ($x = 2$ mm) when the discharge current is appreciable.

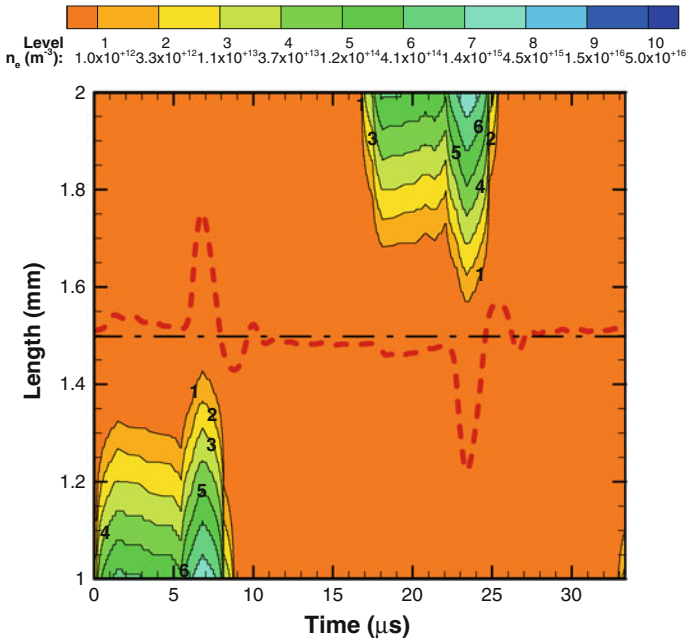

Fig. 8 Spatio-temporal evolution of electron number density

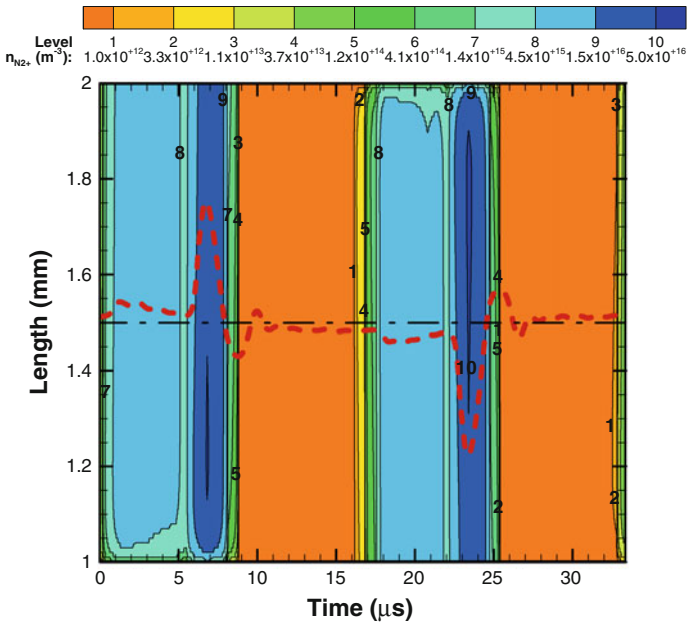

Fig. 9 Spatio-temporal evolution of N_2^+ number density

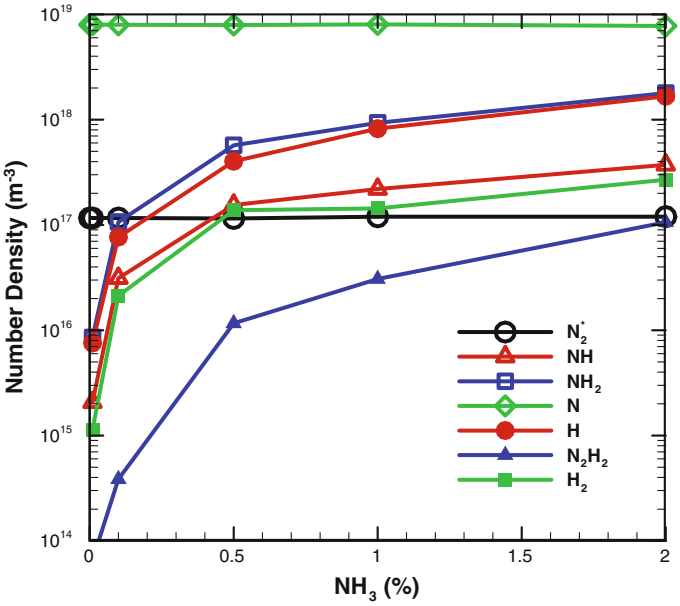

Fig. 10 Cycle-space-averaged number densities of neutral species with concentration ratio of ammonia in AP-DBD

Finally, Fig. 10 presents the cycle-space-averaged number densities of neutral species as a function of ammonia addition. The results show that the most dominant species is atomic nitrogen which had been observed experimentally in pure nitrogen AP-DBD [39] and remains nearly the same no matter how much ammonia is added with the present test condition. Interestingly, metastable nitrogen shows similar trend, although it is approximately 2 orders of magnitude smaller than the atomic nitrogen. The decreasing order of number densities of all neutral species except metastable nitrogen is $N > NH_2 > H > NH > H_2 > N_2H_2$. Abundant atomic nitrogen is generated from three major types of reaction: (1) dissociation of electron-impact on NH, NH_2 and N_2 (No. 14, 21, and 38 in Table 1), (2) de-excited metastable atomic nitrogen (No. 7 in Table 2), and (3) dissociation, recombination and excitation into vibration state of neutral–neutral collision (No. 12, 16, 42, and 48 in Table 3). The number densities of NH_2, H, NH, H_2 and N_2H_2 increase rapidly with increasing addition of ammonia. It is noted that the primary source of NH_2 generation is by electron impact dissociation with ammonia because of low threshold energy of 5.72 eV for dissociation. Abundant generation of NH_2 in N_2/NH_3 discharge plays an important role in incorporating N1 s into some polymer to make it biocompatible [25, 26].

Conclusion

In this study, we have employed one-dimensional self-consistent fluid modeling for simulating a parallel-plate atmospheric-pressure dielectric barrier discharge (AP-DBD, driven by a 30 kHz power source) of nitrogen added with small amount of ammonia (0–2 %). Simulations were validated by good agreement between predicted and experimental

current densities. The simulated results show that the discharges of N_2 mixed with NH_3 (0–2 %) are all typical Townsend-like discharges because the ions always outnumber the electrons to a large extent which leads to no quasi-neutral region in the gap throughout the cycle. N_2^+ and N_4^+ are found to be the most abundant charged species during and after the breakdown process, respectively, like a pure nitrogen DBD. NH_4^+ increases rapidly initially with increasing addition of NH_3 and levels off eventually. In addition, N is the most dominant neutral species, except the background species, N_2 and NH_3, and NH_2 and H are the second dominant species, which increase with increasing added NH_3 in the range of added ammonia. Abundant H, NH and NH_2 in a discharge of N_2 mixed with NH_3 may play a critical role in some applications which require functional group incorporation [e.g., 24–26].

Acknowledgments The authors would like to express their gratitude for the financial support provided by National Science Council of Taiwan throughout the research period.

References

1. Barbir F, Gomez T (1997) Int J Hydrogen Energy 22:1027–1037
2. Klemberg-Sapieha J, Kuttel O, Martinu L, Wertheimer M (1991) J Vac Sci Technol A 9:2975–2981
3. Losurdo M, Capezzuto P, Bruno G, Irene E (1998) Phys Rev B 58:15878
4. Arakoni RA, Bhoj AN, Kushner MJ (2007) J Phys D Appl Phys 40:2476
5. McCurdy PR, Butoi CI, Williams KL, Fisher ER (1999) J Phys Chem B 103:6919–6929
6. Golubovskii YB, Maiorov VA, Behnke J, Behnke JF (2002) J Phys D Appl Phys 35:751–761
7. Choi Y, Kim J, Hwang Y (2006) Thin Solid Films 506:389–395
8. Panousis E, Papageorghiou L, Spyrou N, Loiseau J-F, Held B, Clement F (2007) J Phys D Appl Phys 40:4168–4180
9. Massines F, Rabehi A, Decomps P, Gadri RB, Segur P, Mayoux C (1998) J Appl Phys 83:2950
10. Tochikubo F, Chiba T, Watanabe T (1999) Jpn J Appl Phys 38:5244–5250
11. Golubovskii YB, Maiorov VA, Behnke J, Behnke JF (2003) J Phys D Appl Phys 36:39
12. Wang Q, Sun J, Wang D (2009) Phys Plasmas 16:043503
13. Naudé N, Cambronne JP, Gherardi N, Massines F (2005) J Phys D Appl Phys 38:530–538
14. Massines F, Gherardi N, Naudé N, Ségur P (2005) Plasma Phys Control Fusion 47:B577–B588
15. Luo H, Liang Z, Wang X, Guan Z, Wang L (2010) J Phys D Appl Phys 43:155201
16. Mao M, Bogaerts A (2010) J Phys D Appl Phys 43:205201
17. Yang WD, Wang PN, Liu ZP, Mi L, Chen SC, Li FM (2000) J Phys D Appl Phys 33:3223
18. Nagai H, Takashima S, Hiramatsu M, Hori M, Goto T (2002) J Appl Phys 91:2615
19. Morikawa Y, Yasunami S, Chen W, Hayashi T, Uchida T (2001) J Vac Sci Technol A 19:1747
20. Panda S, Wise R, Mahorowala A, Balasubramanium V, Sugiyama K (2005) J Vac Sci Technol B 23:900–907
21. Nishida M, Yukimura K, Kambara S, Maruyama T (2001) J Appl Phys 90:2672–2677
22. Wan G, Yang P, Fu RKY, Yao ZQ, Huang N, Chu PK (2005) J Vac Sci Technol A 23:1346
23. Akhrarov M, Vasil'ev B, Grasyuk AZ, Yastrebkov A (1982) Sov J Quant Electron 12:1326
24. Klages C-P, Grishin A (2008) Plasma Process Polymer 5:368–376
25. Yang YW, Kuo CL, Wen CC, Wu JY, Huang HY, Chiang MH, Wu JS (2010) Paper presented at the 7th international conference on flow dynamics, Sendai, Japan
26. Yang YW, Kuo CL, Wen CC, Wu JY, Huang HY, Chiang MH, Wu JS (2011) Paper presented at the 8th international conference on flow dynamics, Sendai, Japan
27. Hung CT, Chiu YM, Hwang FN, Chiang MH, Wu JS, Wang YC (2011) Plasma Chem Plasma Process 31:1–21
28. Grubert G, Becker M, Loffhagen D (2009) Phys Rev E 80:036405
29. Hagelaar G, Pitchford L (2005) Plasma Sources Sci Technol 14:722
30. LeVeque RJ (2002) Finite volume methods for hyperbolic problems. Cambridge University Press, Cambridge
31. Lin KM, Hung CT, Hwang FN, Smith MR, Yang YW, Wu JS (2012) Comput Phys Commun 183:1225–1236

32. Scharfetter D, Gummel H (1969) IEEE Trans Electron Devices 16:64–77
33. Balay S, Buschelman K, Gropp WD, Kaushik D, Knepley MG, McInnes LC, Smith BF, Zhang H (2009) http://www.mcs.anl.gov/petsc
34. Saad Y, Schultz MH (1986) SIAM J Sci Stat Comput 7:856–869
35. Chiang MH, Liao KC, Lin IM, Lu CC, Huang HY, Kuo CL, Wu JS, Hsu CC, Chen SH (2010) Plasma Chem Plasma Process 30:553–563
36. Massines F, Gherardi N, Naudé N, Ségur P (2009) Eur Phys J Appl Phys 47:22805
37. Kogelschatz U (2010) J Phys: Conf Ser 257:012015
38. Massines F, Ségur P, Gherardi N, Khamphan C, Ricard A (2003) Surf Coat Technol 175:8–14
39. Panousis E, Ricard A, Loiseau JF, Clement F, Held B (2009) J Phys D Appl Phys 42:205201
40. Hayashi M (1990) In: Capitelli M, Bardley J (eds) Nonequilibrium processes in partially ionized gases. Plenum, New York, pp 333–340